Data-Centric Engineering (2022), 3: e14
doi:10.1017/dce.2022.15

CAMBRIDGE UNIVERSITY PRESS

RESEARCH ARTICLE

Intelligent vehicle drive mode which predicts the driver behavior vector to augment the engine performance in real-time

Srikanth Kolachalama* and Hafiz Malik

University of Michigan, Electrical and Computer Engineering, 4901 Evergreen Rd, Dearborn, Michigan 48128, USA
*Corresponding author. E-mail: skola@umich.edu

Received: 28 August 2021; **Revised:** 18 January 2022; **Accepted:** 13 March 2022

Keywords: Adaptive cruise control; deep learning; driver behavior; engine performance; NARX; vehicle drive mode

Abstract

In this article, a novel drive mode, "intelligent vehicle drive mode" (IVDM), was proposed, which augments the vehicle engine performance in real-time. This drive mode predicts the driver behavior vector (DBV), which optimizes the vehicle engine performance, and the metric of optimal vehicle engine performance was defined using the elements of engine operating point (EOP) and heating ventilation and air conditioning system (HVAC). Deep learning (DL) models were developed by mapping the vehicle level vectors (VLV) with EOP and HVAC parameters, and the trained functions were utilized to predict the future states of DBV reflecting augmented vehicle engine performance. The iterative analysis was performed by empirically estimating the future states of VLV in the allowable range of DBV and was fed into the DL model to predict the performance vectors. The defined vehicle engine performance metric was applied to the predicted vectors, and thus optimal DBV is the instantaneous output of the IVDM. The analytical and validation techniques were developed using field data obtained from General Motors Inc., Warren, Michigan. Finally, the proposed concept was quantified by analyzing the instantaneous engine efficiency (IEE) and smoothness measure of the instantaneous engine map (IEM).

Impact Statement

Vehicle drive modes were developed to augment the rider's comfort, safety and reduce fuel consumption. In this research, a novel "intelligent vehicle drive mode" (IVDM) was proposed, embedded with the functionality of obliging the driver's command in all scenarios and predicting the driver behaviour vector (DBV) for future time steps to enhance the vehicle engine performance without increasing the time of trip traversal. IVDM can be activated as a stand-alone application or in conjunction with any other drive modes, accommodating a vehicle speed >25 MPH on a regular terrain profile. The IVDM is most applicable to the vehicles built-in with advanced infotainment and connectivity features, and could potentially emerge as a new feature of the automotive system.

1. Introduction

The first commercial automobile developed by Karl Benz in 1886 consists of less than 100 components and not more than 10 features (Dietsche and Kuhlgatz, 2014). In the current scenario of the automotive

industry, the advancement of vehicle technology has reached the extent of integrating more than 5,000 components supported by 100 features (Sturgeon et al., 2009). All the features developed either enhance the efficiency of the vehicle (e.g., fuel economy drive mode) or augment the human driving experience (e.g., HVAC), which includes safety (e.g., adaptive cruise control (ACC), lane centering, and auto braking) (Zoepf, 2011). The functionality of these features in real-time is automated and integrated into the vehicle, generally categorized into three elements (none, limited, and bounded) user intervention. The first type would include features that function automatically without driver influence (automatic transmission), whereas the second category accommodates limited user intervention that requires drivers' commands to activate (drive modes). The third element shall take up the driver inputs of activation and magnitudes to function, for example, cabin air temperature (CAT), ACC set speed (Zoepf and Heywood, 2012; Chau et al., 2017). Among these features, the vehicle drive mode plays a prominent role in enhancing driving behavior.

In the latest automotive system, 20 drive modes were developed that allow the user to activate in real-time, as shown in Table 1. When deployed, all the modes are integrated and adapt changes to the vehicle functionality, but none intervenes with the driver behavior vector (DBV) (speed, longitudinal acceleration [LOT], lateral acceleration [LAT], yaw rate [YAR], and cabin air temperature [CAT]). The DBV is the user's prerogative in real-time, and it is known that DBV holds more than a 30% share in affecting vehicle engine performance (Boggio-Marzet et al., 2021). Hence, in this research, a novel "intelligent vehicle drive mode" (IVDM) was proposed, which correlates to type 3 feature, which predicts the DBV by obliging the user's command and inputs in real-time to augment the vehicle engine performance. The multiparametric optimization problem was addressed by utilizing the concepts of feature development, deep learning (DL), and optimization criteria (Kolachalama and Malik, 2021). The following article is organized as follows: The feature requirements of IVDM were proposed in Section 2, Section 3 discusses the methodology of real-time data retrieval, and Section 4 defines the metric for vehicle engine performance. The development of DL models was discussed in Section 5, and the prediction of DBV, including the fail-safe algorithm, was presented in Section 6. The results, discussion, and quantifying the performance of the developed concepts are detailed in Sections 7 and 8. Finally, the conclusions were drawn, and future work of this research was outlined.

2. Functionality of IVDM

The core functionality of the intelligent vehicle drive mode (IVDM) is to predict the driver behaviour vector (DBV) in real-time, reflecting optimal vehicle engine performance. The DBV was categorized into three main elements whose magnitudes are the user's choice: speeding behavior (speed, LOT), steering behavior (LAT, YAR), and CAT as shown in Figure 1. In this section, the feature requirements of IVDM were discussed.

- IVDM could be triggered as a stand-alone application or with any integrated drive mode.
- IVDM applies to speeds >25 miles per hour (MPH) and does not relate to parking lots, critical zones, or traffic congestion. The critical zones include construction, accident, or school areas.
- IVDM is most applicable to any vehicle with built-in advanced driver assistance (ADAS), infotainment, and connectivity (AICON) features (e.g., Cadillac vehicles with super and ultra-cruise features).
- IVDM activates the ACC feature to provide controlled LOT and augmented safety to the vehicle.
- IVDM predicts (Adaptive cruise control set speed profile [ACCSSP], cabin air temperature set profile [CATSP]) by optimizing (Engine operating point [EOP], Cabin air temperature operating point [CATOP]), and estimates [LAT, YAR] by assuming ideal steering behavior (ISB). The details of optimal [EOP, CATOP] and ISB were discussed in Section 4.
- Finally, IVDM predicts the DBV in real-time to augment vehicle engine performance. The default time period and range of predicting [ACCSSP, CATSP] = [10 s, 1,000 m] and (allowable vehicle

https://doi.org/10.1017/dce.2022.15 Published online by Cambridge University Press

Table 1. *Vehicle drive modes—Integrated vehicle system.*

Vehicle drive mode	Functionality
All-wheel drive	The All-wheel drive mode provides torque to all four axles and assists traction control, suitable for snow driving (Goodarzi and Esmailzadeh, 2007)
Baja	The Baja mode is activated explicitly during vehicle traversal over desert sand and can accommodate deflated tires to obtain more turnover stability (Sharma et al., 2015)
Crab	The crab mode is activated for rear-steer vehicles to accommodate lateral shifts for speeds under <25 MPH (Cariou et al., 2008)
Custom	The custom mode is limited to the vehicles equipped to sense the terrain (e.g., Cadillac [V] and Corvette [Z]) and allow the user to input the desired behavior
Economy/DFM/AFM	The fuel economy mode is driven by controlled or reduced acceleration and deactivates the ignition for one or more cylinders to reduce the fuel consumption
Fleet	The fleet mode is equipped with infotainment and connectivity features applicable to autonomous, connected vehicles (Baldacci et al., 2008)
Hill descent	This mode is activated automatically when the vehicle encounters a downslope of more than four% and provides controlled deceleration while traversing sudden slopes (Paul et al., 2016)
Hold	The hold mode is more applicable to hybrid and electric vehicles (e.g., Chevy volt), which retains the battery's state. This feature assists the vehicle to use the battery power optimally, especially when the battery charge is at a higher limit (Chau et al., 2016)
Mountain	Mountain mode is similar to the hill descent mode, which provides stability and controlled acceleration on the contrast while climbing uphill (Slope > 14%) (Paul et al., 2016)
Off-road	The off-road mode is commonly used for rugged navigation, resulting in poor surface contact and low traction (Taghavifar and Mardani, 2017)
Personal	The personal drive mode integrated into the vehicle system allows the driver to set the maximum allowable speed and teen driver limitations (Davis, 2019)
Power	The power mode produces higher torque by accommodating necessary changes in real-time, including reducing the ride height (Zhang and Mi, 2011)
Shuttle	Shuttle mode is most applicable to the transit vehicles used for delivery (Chen et al., 2019)
Snow/Ice	This mode is activated in real-time to provide intelligent traction control for slippery roads and augments the safety of the vehicle system
Sport	The sport mode provides higher torque and throttle response, robust suspension, and stiffer steering, which provides additional stability (Melman et al., 2021)
Stealth	The stealth mode activation is not advisable for inexperienced and low confident drivers. This mode reduces the level of interior illumination to assist night driving (Zou et al., 2012)
Terrain/Crawl	The terrain mode is activated for uneven surfaces to improve traction, stability, and control vehicle traverse (Taghavifar and Mardani, 2017)
Tour/Normal	The touring mode is activated under normal driving conditions, which can function with All-wheel drive and fuel economy modes to optimize the vehicle performance (Lairenlakpam et al., 2018)

Continued

https://doi.org/10.1017/dce.2022.15 Published online by Cambridge University Press

Table 1. *Continued*

Vehicle drive mode	Functionality
Tow/Haul	Haul mode is a customer choice used for logistical purposes for traversing heavy goods and towing (Gao et al., 2015)
Track	The track mode is developed for circuits and tracks with known geometry, providing a more aggressive transmission shift pattern than the sport mode (Onder and Geering, 1995)
Trailer	This mode is activated when a trailer is attached to the vehicle to control the entire system's longitudinal and lateral dynamics (Hac et al., 2008)

Source: General Motors Inc.

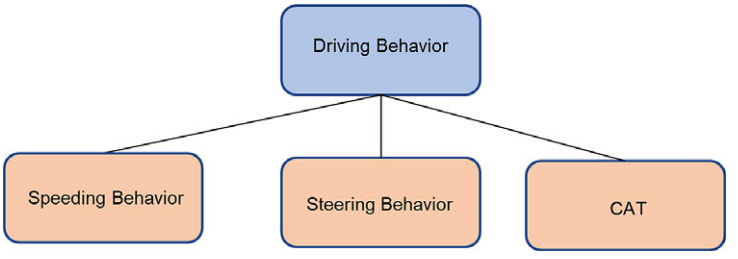

Figure 1. *DBV—predicted elements by IVDM.*

speeds [AVS], allowable vehicle cabin air temperatures [AVC]), whose details were discussed in Section 6.

2.1. Speeding behavior

The proposed functionality IVDM activates the ACC feature when triggered; thus, the ACC controller automatically estimates the parameter LOT based on the ACCSSP (Labuhn and Chundrlik, 1995) and possesses the capability to reduce the vehicle speed while encountering a host vehicle in the defined proximity (Marsden et al., 2001). The ACC feature is a primary component of ADAS which can be activated for any speed ≥25 MPH, resulting in augmented safety and vehicle engine performance (Luo et al., 2010). Thus, IVDM predicts ACCSSP based on the type of road segment (Supplementary Table S8) and further details were discussed in Section 6 (Kolachalama and Malik, 2021a,b).

2.2. Steering behavior

The steering behavior vector (SBV) consists of four elements (speed, LAT, YAR, radius of road curvature [RRC]), and the parameter RRC is known from the AICON feature based on the global position system (GPS) coordinates. The measure of hard braking and acceleration (Wåhlberg, 2007) was extended by introducing the concept of ideal steering behavior (ISB) (Kolachalama et al., 2018). Hence, IVDM would incorporate ISB and the guidelines established by the United States transportation authority to estimate [LAT, YAR] for definite RRC (Kolachalama and Lakshmanan, 2021). The ISB was defined assuming no lateral or longitudinal slip, and the corresponding mathematical models were shown in Section 4.1.

https://doi.org/10.1017/dce.2022.15 Published online by Cambridge University Press

2.3. Cabin air temperature

In an internal combustion engine vehicle, the thermal energy produced by the fuel combustion is exchanged between the environment (external air temperature [EAT]) and the vehicle (Borman and Nishiwaki, 1987). Among the vehicle's many features, the HVAC is the only system that maintains the set cabin air temperature (CAT), driven by user command. The CAT is increased by extracting heat from the engine surface and decreased by the known process of HVAC. Hence, IVDM proposes a model that can generate an optimal CATSP, potentially augmenting the efficiency of HVAC and Engine (Kolachalama and Malik, 2021a,b).

3. Data Retrieval

In order to develop the computational model of IVDM, the real-time testing was performed using Cadillac vehicle segments (2019 XT6, 2021 CT4, 2020 CT5, 2021 Escalade All wheel drive, 2021 Escalade ESV), and the vehicle data was retrieved by applying the principles of the integrated vehicle controller area network bus architecture (Johansson et al., 2005). The test cases were developed by activating ACCSSP in the range [25 85] MPH, targeting all the road segments shown in Supplementary Table S8 and Figure 2. The tools neoVI, Fire 2 (hardware) and Vehicle Spy (software), were utilized to selectively retrieve the signal data for analysis (Figure 3; Jaynes et al., 2016). The data retrieval was done with a default frequency of 10 Hertz (1 time-step = 10 ms), and the properties of the data sets were depicted in Supplementary Tables S1–S7. The elements (vehicle level vectors [VLV], engine operating point [EOP], cabin air temperature operating point [CATOP]) were collected under normal driving conditions for every test case considering the two scenarios, external air temperature EAT > 65°F and EAT <45°F (Supplementary Table S9) whose properties were detailed in below subsections (Kolachalama and Malik, 2021a,b).

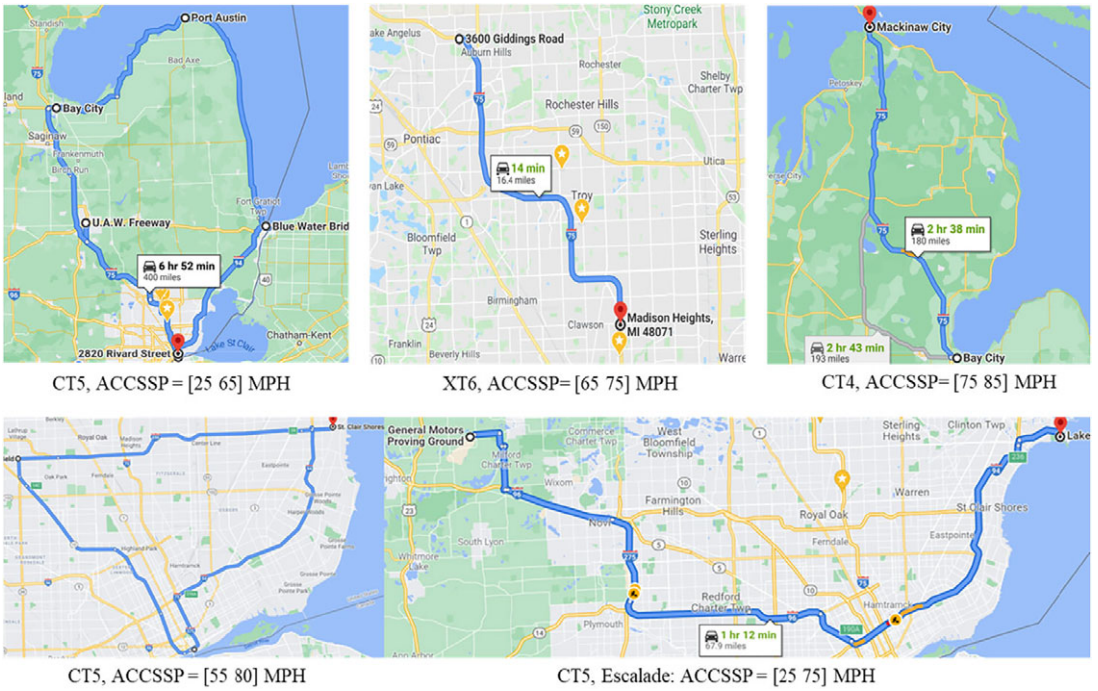

Figure 2. *Cadillac: path traversed—Michigan, USA.* Source: *Google maps; Kolachalama and Malik, 2021a,b.*

https://doi.org/10.1017/dce.2022.15 Published online by Cambridge University Press

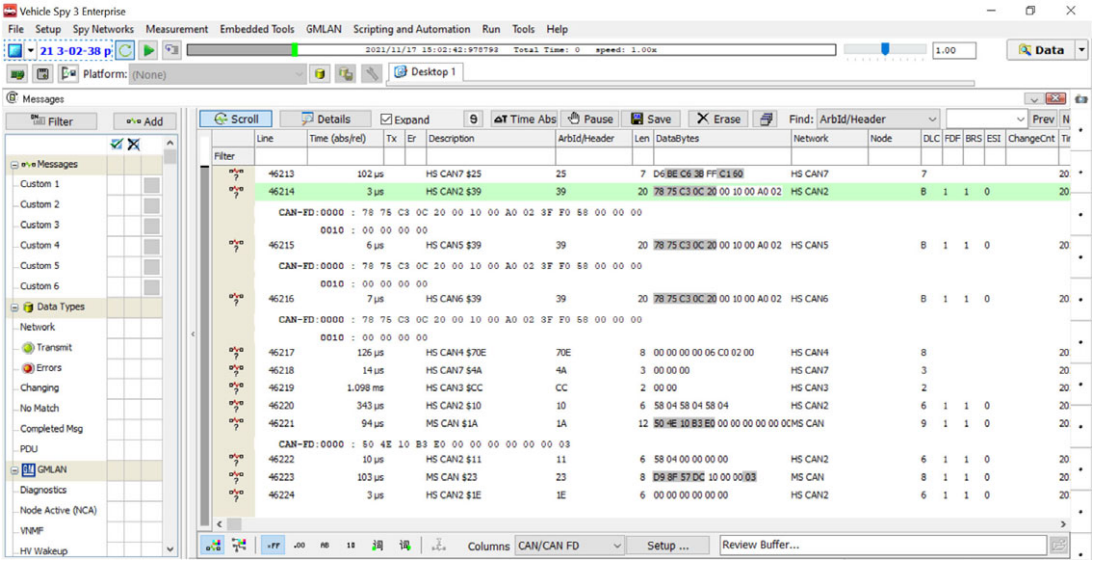

Figure 3. *Controller area network data retrieval—vehicle Spy user interface. Source: General Motors Inc., Detroit, MI.*

3.1. Vehicle level vectors

The VLV include three components, namely, body module, driver behavior, and environmental factors. The body module vector is embedded with the age of the vehicle (time step, odometer), tire pressure, the shape of the vehicle (aerodynamic drag), and load (trailer, passengers). The tire pressure and external load affect the normal and traction forces exerted on the wheels, affecting the vehicle engine performance (Liang et al., 2019). The body design influences aerodynamic resistance and instantaneous fuel consumption rate (IFCR 1E-8 m^3/s) (Sudin et al., 2014), whereas the DBV consists of the elements discussed in Section 2. The environmental factors consist of interactive vehicle elements while traversing any terrain; EAT influences the Engine's thermal stress (Kolachalama et al., 2008), whereas the terrain data (curvature and gradient) obtained from the AICON features affect vehicle dynamics. Also, the gradient is proportional to the vehicle's Euler angles; hence, there is no loss of generality in considering pitch, roll, and yaw angles as inputs replacing the gradient (Eathakota et al., 2010). The parameters steering angle, humidity (HUM), and atmospheric pressure (ATP) were not included in this research as the data has no significant variance, and the effect of these elements on vehicle engine performance is minimal. The real-time analysis was performed under no-slip conditions, that is, the traction force generated at the wheels is proportional to the normal forces (Eathakota et al., 2008).

3.2. Engine operating point

The only external input in an internal combustion engine-driven vehicle is the air-fuel mixture ignited to produce downward thrust onto the piston surface. The flame impingement produces instantaneous engine torque (IET Nm) and is transmitted to the engine components, which results in instantaneous engine speed (IES rad/s). It is a well-established industrial methodology to represent the EOP with the three parameters IET, IES, and IFCR projected on the engine map generated for every vehicle (Kolachalama and Lakshmanan, 2021). Thus, optimal EOP was considered as the criteria to predict ACCSSP, whose details are presented in Section 4.2.

https://doi.org/10.1017/dce.2022.15 Published online by Cambridge University Press

3.3. HVAC parameters: CATOP

The HVAC functionality is driven by multiple parameters: engine fan speed, load, air conditioning refrigerant fluid pressure (ACRFP), engine surface temperature (EST), and power consumed. The analysis of data retrieved resulted in substantial variations of [EST (°F), ACRFP (PSI)] with changes in CAT (°F) and EAT (°F), thus remaining HVAC elements were not considered in this research. The vector [EST (°F), ACRFP (PSI)] is empirically termed as CATOP, and optimal criteria to generate the CATSP was defined in Section 4.3. The snippets of HVAC elements were collected at a frequency of 10 m (odometer reading), as it was observed that the controller area network bus would require at least 300 ms to record variations in CAT (°F) during the steady-state (Kolachalama and Malik, 2021a,b).

4. Vehicle Engine Performance: Criteria

This section defines the concept of ideal steering behavior (ISB), optimal engine and cabin air temperature operating points [EOP, CATOP] reflecting augmented vehicle engine performance.

4.1. Ideal steering behavior

The steering behavior of the vehicle was estimated by the concept ideal steering behaviour (ISB) using the steering behaviour vector [SBV] (speed, LAT, YAR, RRC) (Kolachalama and Malik, 2021a,b). The mathematical model of ISB was defined by Equations (1) and (2), assuming no lateral and longitudinal slip. Equation (1) is a quadratic function relating the parameters of SBV, and Equation (2) is the linear optimization function (LOF) framed to resolve Equation (1). Therefore, [LAT (L_a), YAR (Y_a)] = [0, 0] for high RRC (~∞), and it is easy to see that LOF (~0) has an infinite set of solutions that satisfy the constraint $RRC \cdot Y_a^2 = L_a$. Hence, the parameters [LAT, YAR] could be estimated if the speed value (V_s) is known, and the details were presented in Section 6:

$$2RRC = \frac{V_s^2}{L_a} + \frac{V_s}{Y_a}, V_s = \frac{-L_a + \sqrt{L_a^2 + 8RRC \cdot L_a \cdot Y_a^2}}{2.Y_a}, \tag{1}$$

$$LOF = min[abs(Y_a \cdot V_s - L_a)]. \tag{2}$$

4.2. Engine performance

This research measures the Engine's capability by three parameters (engine torque caliber [ETC], engine speed caliber [ESC], Euclidean distance [ED]), directly related to vehicle engine performance. These parameters represent the torque produced per unit of fuel consumption (ETC), speed produced per unit torque (ESC), and the ED of the EOP from Ideal EOP under normal driving conditions. An engine map is a traditionally accepted convolute graph in the industry, plotted with operating EOP's calibrated at the manufacturing plant. The coordinate with the lowest IFCR (1E-8 m^3/s) was assumed to be the ideal EOP, and the line segment conjoining the operating and ideal EOP was empirically defined as the vehicle engine performance vector. In Sections 5 and 6, the predictive model of [EOP, ACCSSP] was discussed, and Figure 4b is the pictorial representation of the instantaneous engine map (IEM), categorizing two ACCSSP profiles (predicted and constant). The magnitude of the vehicle engine performance vector represents the ED (Equation (3)), and IES (rad/s) was ignored in estimating the ED, as higher IES is desired to reduce the trip time (Kolachalama and Malik, 2021a,b).

Vehicles traversing arterial road segments with speed limits ranging [25 45] MPH have operating EOP closer to the ideal EOP (lower ED), as shown in the engine map (Figure 4a). The speeds of the vehicles on freeways range [65 85] MPH, which correspond to higher IES, and fluctuating [IET, IFCR] depending on the dynamic state of the vehicle. Also, the state ways with speed limits (SL) as [45 65] MPH are

https://doi.org/10.1017/dce.2022.15 Published online by Cambridge University Press

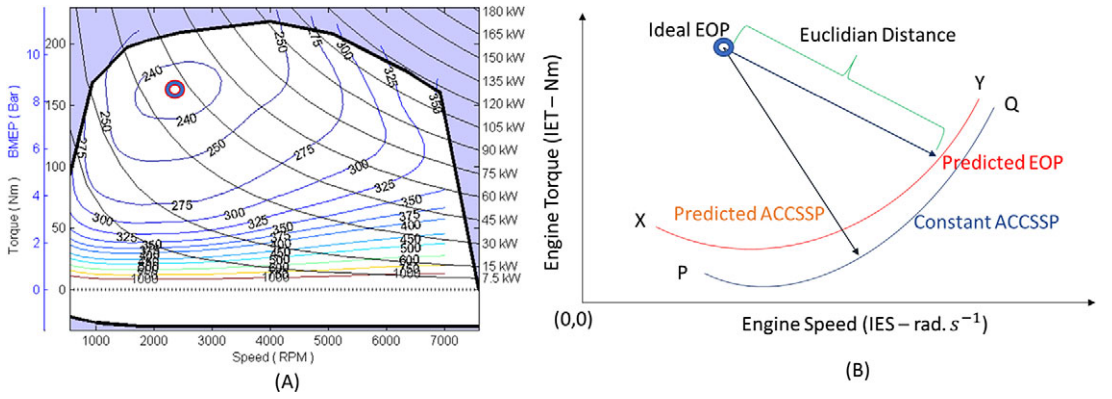

Figure 4. *(a) Engine map: 2007 Toyota Camry 2.4 L I4 and (b) IEM—vehicle engine performance vector (Kolachalama and Malik, 2021a,b).* Source: *Ricardo baseline standard car engine: Tier 2 fuel. EPA ALPHA vehicle simulations. Version: June 20, 2016. The engine map for the 2007 Toyota Camry 2.4 L I4, whose ideal EOP = [170 Nm, 2,400 RPM, 230 g/kwhr], was shown in (a). The conversion to the SI units was performed assuming the [Calorific value (C_v), density (ρ_f)] = [45 MJ/kg, 750 kg/m^3], and thus the ideal EOP = [170 Nm, 251.33 rad/s^1, 159 1E-8 m^3/s]. A 2020 Cadillac CT5 test vehicle was utilized in the current research (Section 6), whose ideal EOP was assumed to be [250 Nm, 140 rad/s, 180 1E-8 m^3/s].*

considered the green zone (low IFCR). Hence, the generic criteria for augmented Engine operating conditions would be lower [ED, IFCR] and higher [IET, IES, ETC, ESC]:

$$ED = \sqrt{(IET_i - IET_k)^2 + (IFCR_i - IFCR_k)^2}, \tag{3}$$

$$\text{ETC} = \frac{IET}{IFCR}, \tag{4}$$

$$\text{ESC} = \frac{IES}{IET}. \tag{5}$$

4.3. HVAC criteria: CATOP

In this research, the elements [Engine surface temperature (EST), air conditioning refrigerant fluid pressure (ACRFP)] were defined as CATOP, and the optimal thermal stress and engine oil viscosity on the engine components result when EST (EST_i) = 194°F (Borman and Nishiwaki, 1987). The parameters A1 and A2, shown in (6) and (7), represent the conformance between the operating EST (EST_o) and ideal EST (EST_i). Hence, minimum values of A1 and A2 are the criteria for optimal HVAC. The retrieved data are shown in Supplementary Tables S1–S7, which depict the recorded EST ranges [165 220]°F.

The refrigerant integrated into the air conditioning system (ACS) of the Cadillac vehicle was assumed to be R134a, and augmented functionality of ACS was achieved by limiting the maximum value of operating ACRFP (ACRFP_o). The upper boundary limits of ACRFP (ACRFP_h) were defined in Supplementary Table S10 in correlation with the EAT, and the intermittent boundary values of ACRFP (PSI) for EAT = [65 110]°F were estimated by basic linear interpolation. Therefore, minimum B defined in (8) and (9) was considered the optimal HVAC criterion corresponding to ACRFP (PSI) (Kolachalama

https://doi.org/10.1017/dce.2022.15 Published online by Cambridge University Press

and Malik, 2021a,b). Thus, B is always nonnegative when EAT ≥ 65°F, but when EAT <65°F, the parameter B is not significant in our analysis:

$$A1 = (EST_o - EST_i),\ if\ EST_o > EST_i = 194°\text{F}, \tag{6}$$

$$A2 = (EST_i - EST_o),\ if\ EST_o \leq EST_i = 194°\text{F}, \tag{7}$$

$$B = (ACRFP_o - ACRFP_h),\ if\ ACRFP_o > ACRFP_h(\text{PSI}), \tag{8}$$

$$B = 0,\ if\ \text{ACRFP}_o \leq \text{ACRFP}_h \text{or} EAT < 65°\text{F}. \tag{9}$$

4.4. Smoothness measure: Vehicle engine performance

The elements of the EOP were analyzed and it was observed that IES (rad/s^1) is a smoother curve, whereas [IFCR, IET] have fluctuating behavior. The flame propagation phenomena due to the ignition of the fuel-air mixture trigger thrust and torque with oscillating magnitudes. Hence to minimize the vibrations, techniques include optimizing the spark ignition timing and camshaft mechanism (Kakaee et al., 2011), integrating flywheel and generator (Gusev et al., 1997) were adopted. Therefore, smoothness measure vector (SMV) [R^2, adjusted R^2, sum of square errors (SSE), root mean square error (RMSE)] of the parameters—[EOP, CATOP] and [ED, ETC, ESC] was considered in our analysis, and the vehicle engine performance criteria were shown in Supplementary Table S11 (Kolachalama and Malik, 2021a,b). The SMV was estimated using the built-in toolboxes of MATLAB, and the spline function was utilized to fit the data points.

5. DL Models: Prediction of [EOP, CATOP]

The proposed IVDM, when activated, predicts the DBV elements [ACCSSP, CATSP] by optimizing the vectors [EOP, CATOP] and estimates [LAT, YAR] utilizing ideal steering behavior (ISB). In this section, individual supervised predictive models were developed for five Cadillac (CT4, CT5, Escalade All wheel drive, Escalade ESV, XT6) vehicle lines by mapping the vehicle level vectors (VLV) with the elements [EOP, CATOP] as shown in Figure 5. The retrieved data were analyzed as time-sensitive; thus, Auto-regressive Network with Exogenous Inputs (NARX) and long short-term memory (LSTM) deep learning (DL) methods were the obvious choices of the current research. Hence, in this section, the apt DL model for vehicle data was identified, and performance analysis was conducted using a traditional statistical measure vector (STMV). Autoregressive DL models were not considered in this article because of the limitation on the size of the input vector (Kolachalama and Lakshmanan, 2021).

5.1. NARX and LSTM methods: Modeling

The default properties built-in MATLAB were utilized to initialize the process, as shown in Supplementary Table S12, and DL models were developed using m-script. The NARX is a recurrent dynamic network whose mathematical model predicts the future output steps by regressing the previous states of output and exogenous (independent) inputs. In contrast, LSTM predicts the output by considering the long-term dependencies of the entire set of inputs and possesses the properties of recurrent neural networks (Kolachalama and Lakshmanan, 2021). LSTM produced the best results for classification and regression of biological data (e.g., antibody sequencing), and NARX is preferred for the data with nonlinear behavior. The performance analysis of the predictive model of EOP using NARX and LSTM

https://doi.org/10.1017/dce.2022.15 Published online by Cambridge University Press

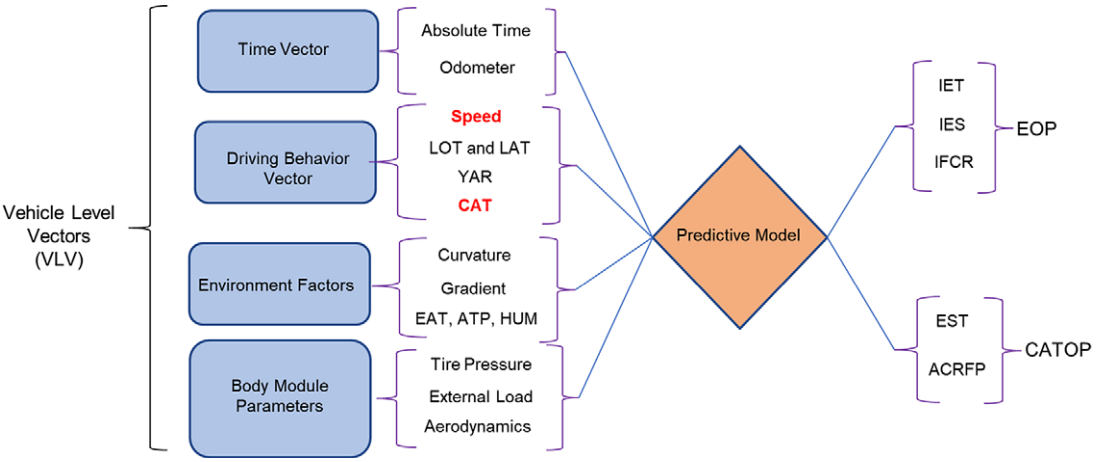

Figure 5. *NARX DL predictive models: EOP and CATOP—Inputs and outputs (Kolachalama and Malik, 2021a,b).*

DL methods was done by varying the parameters (training size, test size, hidden layers/units), and it was proven that the NARX method outperformed LSTM for ACC activated and deactivated datasets (Kolachalama and Lakshmanan, 2021). In this section, extended validation was performed using a similar methodology for the datasets depicted in Supplementary Tables S1–S7.

5.2. NARX and LSTM methods: Performance analysis

The resulting plots compare the retrieved data (blue) and predicted values (orange) using [NARX, LSTM] methods for randomly selected snippets as shown in Supplementary Figures S1–S6 (NARX) and Supplementary Figures S7–S12 (LSTM). The first row of the figure represents the three elements of EOP, and the units of [IET, IES] were Nm and rad/s, whereas IFCR was recorded on a scale of 1E-8 m^3/s. The second row consists of the CATOP vector [Engine surface temperature (EST), air conditioning refrigerant fluid pressure (ACRFP)], measured in [Fahrenheit (°F), pounds per square inch (PSI)]. The numerical performance of the developed deep learning (DL) models was validated by adopting traditional statistical measure vector (STMV) = [root means square error (RMSE), first-order derivative (FOD), signal-to-noise ratio (SNR)] on the conformance between actual and predicted values, as shown in Supplementary Tables S13 and S14. The NARX method produced maximum RMSE IET = 2.465 (CT4—Set 1), whereas LSTM network produced minimum RMSE IET = 18.515 (XT6—Set 2). The element IES was predicted with equal competence by NARX (FOD < 1.129) and LSTM (FOD < 1.42), but LSTM lacked the required consistency savvy (mean IFCR FOD = 11.9) to match the NARX output (mean IFCR FOD = 10.22) for all the datasets. Similarly, the NARX prediction had 75% lower RMSE EST and 18% lower FOD ACRFP when compared to LSTM output. It is easy to see that, despite the stochastic variation, the predicted curves aligned to the actual values, and by visualizing the fit of NARX prediction is smoother when compared with LSTM graphs and thus, the SNR results play a low priority role.

The research scope was limited to a single-vehicle test case leveraging the 2020 Cadillac CT5 datasets (Supplementary Tables S4–S7). Hence, specific snippets of data with ACCSSP = [30 75] MPH (Supplementary Table S15) were selected, and another validation check was performed for the developed NARX DL model. The plots of predicted [EOP, CATOP], comparing the actual values, were shown individually in Supplementary Figures S13–S17, Supplementary Figures S18–S22 (EAT > 65 °F), and Supplementary Figures S23–S27 (EAT < 45°F). The computational efficacy of prediction was projected using the STMV, as shown in Supplementary Tables S16 and S17. The IET RMSE values were <1.7, and IES FOD was <0.27 for all the datasets, whereas the IFCR SNR has an acceptable range of [6.36 985.73]. Similarly, the EST RMSE <2.3 (EAT > 65°F) and <0.9 (EAT <45°F), whereas ACRFP SNR has a range of

https://doi.org/10.1017/dce.2022.15 Published online by Cambridge University Press

[2.2 16.1]. Therefore, the efficacy of the NARX DL model was proven, and the results were assumed to be satisfactory. Also, an increased number of datasets and enhanced validation would enrich prediction precision. However, in this article, the core concept of IVDM was highlighted, and further elements of the research were pursued in Sections 6–9.

6. Prediction of DBV

The steps applicable to IVDM—prediction of DBV utilizing the functionality (Section 2), datasets (Section 3), criteria (Section 4), and deep learning (DL) models (Section 5), were defined in this section. The prediction of DBV elements [ACCSSP (MPH), CATSP (°F)] was made by the four-step process described in Figure 6, and the applicable equation sets are shown in Table 2. The ACCSSP (>25 MPH) was predicted by optimizing EOP assuming constant CAT; and similarly, CATSP (°F) was predicted by optimizing CATOP and resulted ACCSSP in the previous step (Kolachalama and Malik, 2021a,b). The default range of [allowable vehicle speeds (AVS), allowable cabin air temperatures (AVC)] to predict [ACCSSP, CATSP] was estimated by the relations (10) and (11), assuming [DCAT, EAT_o] = [70, 65]°F. The ADAS, infotainment, and connectivity (AICON) features retrieve the speed limits of the road segments (SL) in real-time, and the functionality of the SIGN mathematical model was utilized, to estimate AVC = [65 70]°F (EAT ≥ EAT_o°F) or [70 75] °F (EAT < EAT_o°F):

$$\text{AVS} = [\text{Speed Limit-5}, \text{Speed Limit} + 5]\,\text{MPH}, \tag{10}$$

$$\text{AVC} = [MinCAT, MaxCAT]°\text{F}, \tag{11}$$

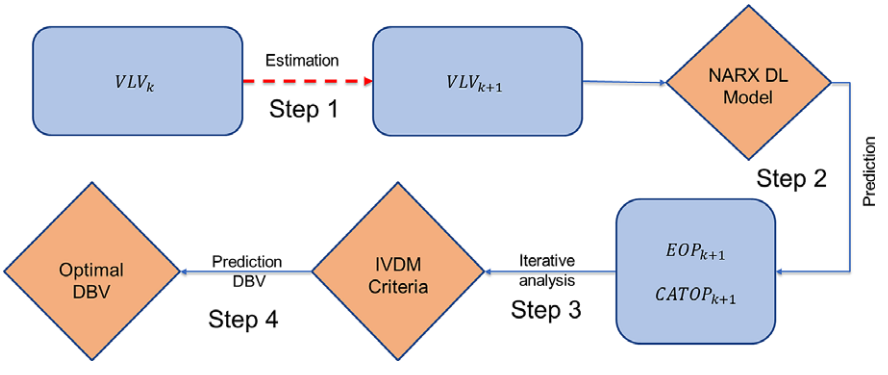

Figure 6. *IVDM—prediction of DBV (Kolachalama and Malik, 2021a,b).*

Table 2. *IVDM equation set—Prediction of DBV (Kolachalama and Malik, 2021a,b).*

$T_{k+1} = T_k + dT$	$2\text{RRC}_{k+1} = \frac{S_{k+1}^2}{L_{a(k+1)}} + \frac{S_{k+1}}{Y_{a(k+1)}}$, $\min\left[\text{abs}\left(Y_{a(k+1)}.S_{k+1} - L_{a(k+1)}\right)\right]$	$\text{EAT}_{k+1} = \text{EAT}_k$
$O_{k+1} = O_k + S_k.dT$	$L_{o(k+1)} = g\mu_r + g\sin\left(\theta_{g(k+1)}\right) + \frac{\rho_a C_d.A_c}{2.(M_c+M_L)}.S_{k+1}^2$	$\text{TP}_{k+1} = \text{TP}_k$
$S_{k+1} = [65, 75]$ MPH	$\text{CAT}_{k+1} = \text{CAT}_k$ *or* $[65\ 70]°F$ *or* $[70\ 75]°F$	Gravity (g) = 9.81 m/s^2
$C_d = 0.31$; $A_c = 1.71$ m^2	Mass of the vehicle M_c=1,769.69 kg,	Rolling coefficient μ_r= 0.013
$\rho_a = 1.225$ kg/m^3	Mass of the external load M_L=78.7 kg	

https://doi.org/10.1017/dce.2022.15 Published online by Cambridge University Press

$$MinCAT = min\,[DCAT - 5x; DCAT + 5x]; MaxCAT = max\,[DCAT - 5x; DCAT + 5x],$$

$$x = SIGN\,(EAT - EAT_o).$$

6.1. Estimation of future input states: Vehicle level vectors

Step 1: The empirical relations defined in Table 2 were utilized to estimate the future input values of vehicle level vectors (VLV_{k+1}) of the DL model relative to the current state of the vehicle (VLV_k) (Figure 5). The speed (S_{k+1}) was varied in the default range of AVS, and the parameter odometer (O_{k+1}) was calculated by basic linear interpolation using [S_{k+1}, $L_{o(k+1)}$] assuming a constant time-step. The magnitude of LOT ($L_{o(k+1)}$) was estimated by calculating the force required to overcome the resistance (rolling, gradient, aerodynamics) for maintaining the ACCSSP, assuming no-slip and tire pressure TP_{k+1} is same as the previous step measured in kilopascals (kPa). The rolling resistance was estimated using the coefficient (μ_r), whereas aerodynamic resistance is calculated using the area of cross section, drag coefficient, and density of air [A_c, C_d, ρ_a] whose magnitudes were shown in Table 2. The steering parameters [LAT ($L_{a(k+1)}$),YAR ($Y_{a(k+1)}$)] were estimated assuming ISB, whereas the cabin air temperature $CAT_{k+1}$is varied in the default range of AVC. The Cadillac is equipped with [ADAS, AICON] features (super and ultra-cruise), which would generate the vectors [RRC, gradient, EAT] = [RRC_{k+1}, Θ_{k+1}, EAT_{k+1}] based on the GPS coordinates, and thus VLV_{k+1} was estimated as shown in Table 3.

6.2. Prediction of output states: NARX DL model

Step 2: The input sets of vehicle level vectors (VLV_{k+1}) were estimated for all the values of the AVS range (e.g., [65, 75] MPH), and thus 11 sets of inputs were generated. These matrices were fed into the developed NARX DL model, and therefore a corresponding 11 sets of EOP_{k+1} were predicted. Similarly, six sets of $CATOP_{k+1}$ were predicted by varying the Cabin air temperatures in the allowable range AVC = [65 70]°F.

Table 3. *Estimated inputs—deep learning model (10 time steps = 1 s) (Kolachalama and Malik, 2021a,b).*

Time step	Odometer (miles)	Speed (MPH)	RRC (m)	YAR (rad/s)	LAT (m/s^2)	LOT (m/s^2)	EAT (°F)	CAT (°F)
T_0	1,000.000	[65 75]	8,304.140	0.216	0.118	0.438	[78.3], [40.1]	[65 70], [70 75]
dT_{10}	1,000.002	[65 75]	8,304.140	0.216	0.118	0.375	[78.3], [40.1]	[65 70], [70 75]
dT_{20}	1,000.004	[65 75]	8,304.140	0.216	0.118	0.313	[78.3], [40.1]	[65 70], [70 75]
dT_{30}	1,000.006	[65 75]	9,342.158	0.192	0.105	−0.125	[78.3], [40.1]	[65 70], [70 75]
dT_{40}	1,000.008	[65 75]	24,912.420	0.072	0.039	−0.188	[78.3], [40.1]	[65 70], [70 75]
dT_{50}	1,000.010	[65 75]	74,737.261	0.024	0.013	−0.063	[78.3], [40.1]	[65 70], [70 75]
dT_{60}	1,000.012	[65 75]	74,737.261	0.024	0.013	0.250	[78.3], [40.1]	[65 70], [70 75]
dT_{70}	1,000.014	[65 75]	37,368.631	0.048	0.026	0.250	[78.3], [40.1]	[65 70], [70 75]
dT_{80}	1,000.016	[65 75]	24,912.420	0.072	0.039	0.188	[78.3], [40.1]	[65 70], [70 75]
dT_{90}	1,000.018	[65 75]	24,912.420	0.072	0.039	0.188	[78.3], [40.1]	[65 70], [70 75]
T_1	1,000.019	[65 75]	9,342.158	0.192	0.105	0.313	[78.3], [40.1]	[65 70], [70 75]

https://doi.org/10.1017/dce.2022.15 Published online by Cambridge University Press

6.3. Implementation: Vehicle engine performance criteria

Step 3: The vehicle engine performance criteria defined in Section 4 were applied to the predicted vectors $[EOP_{k+1}, \mathrm{CATOP}_{k+1}]$, whose results for 10 time-steps were shown in Tables 4 and 5. The top six performing optimal ACC speeds and CAT's were selected for each vehicle engine performance criteria, as shown in Tables 6 and 7. Among these values, the top three modes were selected as the eligible vehicle speeds (EVS) [71, 70, 69] MPH and eligible vehicle cabin air temperatures (EVC) ([68, 70, 67]°F or [72, 71, 70]°F) for the time step T_{k+1}. A similar process was implemented for 100-time steps, and therefore the [ACC Speed, CAT] matrix was framed as shown in Table 8.

6.4. Algorithm: [ACCSSP, CATSP] prediction

The [ACC, CAT] matrix was framed with three [EVS, EVC] for 10-time steps [1 s, 100 m]. Thus, a maximum of 3^{10} [ACCSSP's, CATSP's] are possible for 100-time steps, and a unique [ACCSSP, CATSP] was generated by implementing the following algorithm.

Step 4A: Estimation of ACCSSP

1. Assuming the [ACC speed, Speed limit] at T_k is $[S_k, \mathrm{SL}]$, and if the EVS at T_{k+1} are either S_k+1, S_k, or S_k-1, then $S_{k+1} = S_k+1$.
2. If the EVS at T_{k+1} is neither S_k+1, S_k, nor S_k-1, then $S_{k+1} = S_k$.
3. If $S_{k+1} = S_k$ for more than 100-time steps, $S_{k+1} = S_k+1$ if $S_k+1 \leq \mathrm{SL}+5$ or $S_{k+1} = S_k-1$ if $S_k = \mathrm{SL}+5$.

Step 4B: Estimation of CATSP

1. Assuming the CAT at dT_k is C_k, if the EVC at dT_{k+1} are either C_k+1, C_k, or C_k-1.

   Case 1: $EAT_k \geq EAT_o$°F, then $C_{k+1} = C_k+1$. ($C_k+1 \leq maxCAT$°F).

   Case 2: $EAT_k < EAT_o$°F, then $C_{k+1} = C_k-1$. ($C_k-1 \geq minCAT$°F)

2. If the EVC at dT_{k+1} are neither C_k+1, C_k, nor C_k-1, then $C_{k+1} = C_k$. ($minCAT$°F $\leq C_k \leq maxCAT$°F)
3. If $C_{k+1} = C_k$ for more than 100-time steps, then

   Case 1: $EAT_k \geq EAT_o$°F, then $C_{k+1} = C_k+1$, if $C_k+1 \leq maxCAT$°F or $C_{k+1} = C_k-1$, if $C_k = maxCAT$°F.

   Case 2: $EAT_k < EAT_o$°F, then $C_{k+1} = C_k-1$, if $C_k-1 \geq minCAT$°F or $C_{k+1} = C_k+1$, if $C_k = minCAT$°F.

The algorithm proposed in Step 4 [A, B] was implemented on [ACC Speed, CAT] matrices (Table 8), by unit step increment of $[S_0, C_0]$ in the range of [AVS, AVC]. The possible [ACCSSP's, CATSP's] were shown in Figures 7a and 8a, and a unique [ACCSSP, CATSP] was obtained by assuming initial values of ACC Speed (IAS) and Cabin air temperature (ICAT) [IAS (S_0), ICAT (C_0)] = [70 MPH, 65°F] as shown in Figures 7b and 8b.

7. Results and Validation

The functionality of IVDM was applied to the snippets selected from the 2020 Cadillac CT5 data sets for the ACCSSP = [30 70] MPH. The resulted plots of predicted [ACCSSP, CATSP] implementing all the steps defined in Section 6, for the test cases were depicted in Supplementary Figures S28–S37.

https://doi.org/10.1017/dce.2022.15 Published online by Cambridge University Press

Table 4. *Vehicle engine performance—Iteration of AVS (10 time steps = 1 s).*

Data		ACC speed—Iterative analysis										
EOP	Speed	65	66	67	68	69	70	71	72	73	74	75
IET	Dist	1.6E+04	3.1E+04	4.7E+04	6.2E+04	7.8E+04	9.4E+04	1.1E+05	1.2E+05	1.4E+05	1.6E+05	1.7E+05
	R^2	0.76	0.83	0.77	0.74	0.77	0.77	0.75	0.77	0.75	0.78	0.76
	Adj. R^2	0.4	0.57	0.43	0.36	0.44	0.43	0.39	0.44	0.37	0.44	0.4
	SSE	6.26	4.47	5.94	6.69	5.82	5.94	6.34	5.76	6.49	5.72	6.16
	RMS	0.4	0.33	0.39	0.41	0.38	0.38	0.4	0.38	0.4	0.38	0.39
IES	Area	1.8E+04	3.5E+04	5.3E+04	7.1E+04	8.9E+04	1.1E+05	1.2E+05	1.4E+05	1.6E+05	1.8E+05	2.0E+05
	R^2	1	1	1	1	1	1	1	1	1	1	1
	Adj. R^2	0.99	0.99	0.99	0.99	0.99	0.99	0.99	0.99	1	0.99	0.99
	SSE	0.003	0.002	0.003	0.003	0.003	0.003	0.002	0.001	0.001	0.001	0.001
	RMS	0.009	0.007	0.008	0.008	0.009	0.008	0.007	0.006	0.005	0.006	0.006
IFCR	Area	2.8E+04	5.6E+04	8.4E+04	1.1E+05	1.4E+05	1.7E+05	1.9E+05	2.2E+05	2.5E+05	2.7E+05	3.0E+05
	R^2	0.78	0.78	0.72	0.74	0.8	0.75	0.81	0.74	0.76	0.68	0.67
	Adj. R^2	0.46	0.45	0.31	0.35	0.5	0.37	0.53	0.36	0.4	0.22	0.17
	SSE	4,913.31	4,737.99	5,613.29	4,967.08	3,726.95	4,633.05	3,429.65	4,679.59	4,418.54	5,766.31	6,140.52
	RMS	11.19	10.99	11.97	11.26	9.75	10.85	9.35	10.92	10.62	12.13	12.52
ETC	Area	5.4E+01	1.1E+02	1.6E+02	2.2E+02	2.8E+02	3.3E+02	3.9E+02	4.5E+02	5.0E+02	5.6E+02	6.2E+02
	R^2	0.788	0.781	0.724	0.739	0.802	0.751	0.814	0.745	0.759	0.689	0.671
	Adj. R^2	0.469	0.452	0.309	0.348	0.504	0.377	0.535	0.362	0.398	0.222	0.176
	SSE	0.02	0.02	0.025	0.023	0.017	0.022	0.016	0.023	0.022	0.03	0.033
	RMS	0.022	0.023	0.025	0.024	0.021	0.023	0.02	0.024	0.024	0.028	0.029
ESC	Area	1.1E+02	2.2E+02	3.3E+02	4.5E+02	5.6E+02	6.7E+02	7.8E+02	9.0E+02	1.0E+03	1.1E+03	1.2E+03
	R^2	0.822	0.869	0.824	0.801	0.826	0.817	0.799	0.812	0.783	0.807	0.792
	Adj. R^2	0.554	0.672	0.56	0.503	0.565	0.542	0.497	0.529	0.457	0.517	0.479
	SSE	0	0	0	0	0	0	0	0	0	0	0
	RMS	0.003	0.002	0.003	0.003	0.003	0.003	0.003	0.003	0.003	0.003	0.003
ED	Area	1.9E+04	3.7E+04	5.5E+04	7.2E+04	9.0E+04	1.1E+05	1.2E+05	1.4E+05	1.6E+05	1.7E+05	1.9E+05
	R^2	0.787	0.783	0.725	0.743	0.802	0.751	0.815	0.747	0.761	0.689	0.671
	Adj. R^2	0.467	0.457	0.311	0.358	0.504	0.378	0.538	0.368	0.402	0.222	0.176
	SSE	4,896.87	4,721.42	5,595.32	4,950.75	3,716.68	4,620.39	3,421.22	4,665.06	4,404.92	5,749.95	6,123.26
	RMS	11.18	10.978	11.951	11.241	9.74	10.86	9.345	10.912	10.604	12.115	12.502

Table 5. *Vehicle engine performance—Iteration of AVC (10-time steps = 100 m).*

CAT	A1					A2					B				
°F	Area	R^2	Adj. R^2	SSE	RMSE	Area	R^2	Adj. R^2	SSE	RMSE	Area	R^2	Adj. R^2	SSE	RMSE
ACCSSP = 70 MPH; EAT = 78.75°F															
65	114.5	0.994	0.986	1.495	0.194	1,931	0.998	0.994	61.03	1.242	2,252	0.995	0.989	158.9	2.004
66	175.2	0.995	0.987	2.749	0.264	1,994	0.998	0.994	64.36	1.275	2,365	0.996	0.989	167.8	2.059
67	216.5	0.992	0.979	6.555	0.407	2,020	0.998	0.994	67.47	1.306	2,379	0.996	0.990	149.4	1.943
68	203.8	0.992	0.981	5.391	0.369	1,872	0.997	0.993	67.63	1.307	2,399	0.996	0.990	155.5	1.983
69	178.2	0.993	0.982	3.933	0.315	1,688	0.997	0.993	52.16	1.148	2,402	0.996	0.990	167.6	2.058
70	201.9	0.995	0.986	3.773	0.309	1,612	0.998	0.994	44.56	1.061	2,416	0.996	0.990	162.6	2.027
ACCSSP = 70 MPH; EAT = 38.3°F															
70	47.069	0.990	0.976	0.551	0.118	40.095	0.987	0.968	0.938	0.154	0.000	0.000	0.000	0.000	0.000
71	45.876	0.990	0.975	0.557	0.119	40.662	0.987	0.968	0.961	0.156	0.000	0.000	0.000	0.000	0.000
72	45.408	0.990	0.975	0.561	0.119	41.013	0.987	0.968	0.978	0.157	0.000	0.000	0.000	0.000	0.000
73	45.575	0.990	0.975	0.566	0.120	41.169	0.987	0.968	0.988	0.158	0.000	0.000	0.000	0.000	0.000
74	46.270	0.990	0.975	0.569	0.120	41.162	0.987	0.968	0.993	0.158	0.000	0.000	0.000	0.000	0.000
75	47.368	0.990	0.975	0.572	0.120	41.026	0.987	0.967	0.993	0.158	0.000	0.000	0.000	0.000	0.000

Table 6. *Optimal ACC speeds—Vehicle engine performance (10 time steps = 1 s).*

Area	R^2	Adj.R^2	SSE	RMS	Area	R^2	Adj.R^2	SSE	RMS	Area	R^2	Adj. R^2	SSE	RMS
IET							IES					IFCR		
75	69	69	70	70	75	68	68	75	75	65	66	66	75	75
74	70	70	69	69	74	71	71	71	71	66	69	69	66	66
73	65	65	71	71	73	70	70	68	68	67	75	75	69	69
72	68	68	72	72	72	69	69	70	70	68	65	65	65	65
71	71	71	68	68	71	67	67	72	72	69	70	70	70	70
70	73	73	73	73	70	72	72	74	74	70	67	67	72	72
ETC							ESC					ED		
75	66	66	66	66	75	69	69	70	70	65	66	66	75	75
74	69	69	65	65	74	70	70	69	69	66	69	69	66	66
73	75	75	69	69	73	68	68	71	71	67	75	75	69	69
72	65	65	75	75	72	65	65	72	72	68	65	65	70	70
71	70	70	70	70	71	71	71	73	73	69	70	70	65	65
70	67	67	67	67	70	66	66	68	68	70	67	67	72	72

Table 7. *Optimal CAT values—Vehicle engine performance (10 time steps = 100 m).*

A1					A2					B				
Area	R^2	Adj. R^2	SSE	RMSE	Area	R^2	Adj. R^2	SSE	RMSE	Area	R^2	Adj. R^2	SSE	RMSE
EAT = 78.75°F														
65	66	66	65	65	70	66	66	70	70	70	67	67	67	67
66	70	70	66	66	69	65	65	69	69	69	68	68	68	68
69	65	65	70	70	68	67	67	65	65	68	70	70	65	65
EAT = 38.3°F														
72	70	70	70	70	70	71	71	70	70	70	70	70	70	70
73	71	71	71	71	71	70	70	71	71	71	71	71	71	71
71	72	72	72	72	72	72	72	72	72	72	72	72	72	72

Table 8. *Optimal ACC speed (10 s) and CAT matrix (1,000 m)—100-time steps.*

ACC speed matrix (10 seconds)										CAT matrix (1,000 m)									
T_1	T_2	T_3	T_4	T_5	T_6	T_7	T_8	T_9	T_{10}	dT_1	dT_2	dT_3	dT_4	dT_5	dT_6	dT_7	dT_8	dT_9	dT_{10}
69	68	66	75	74	67	67	75	67	75	67	70	67	65	66	65	68	67	65	69
71	70	65	68	72	71	72	66	75	71	65	67	70	69	67	70	65	69	66	68
68	71	67	65	65	74	73	68	73	65	70	68	68	67	65	69	66	65	68	67

https://doi.org/10.1017/dce.2022.15 Published online by Cambridge University Press

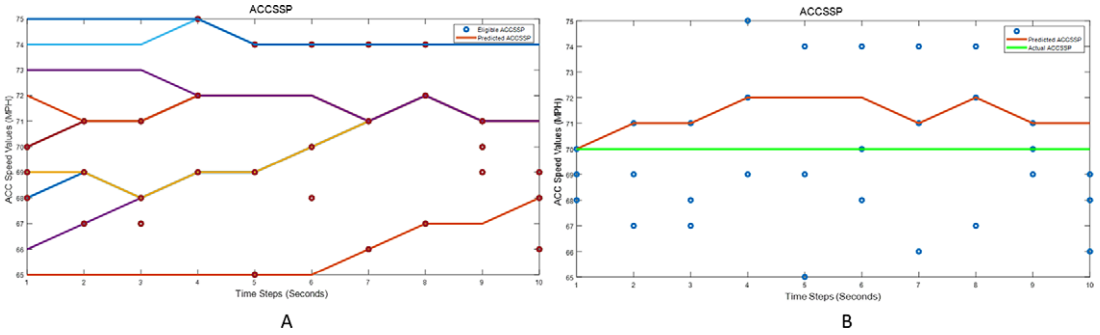

Figure 7. *Unique ACCSSP generation—(a) AVS = [65 75] MPH and (b) Initial ACC speed = 70 MPH.*

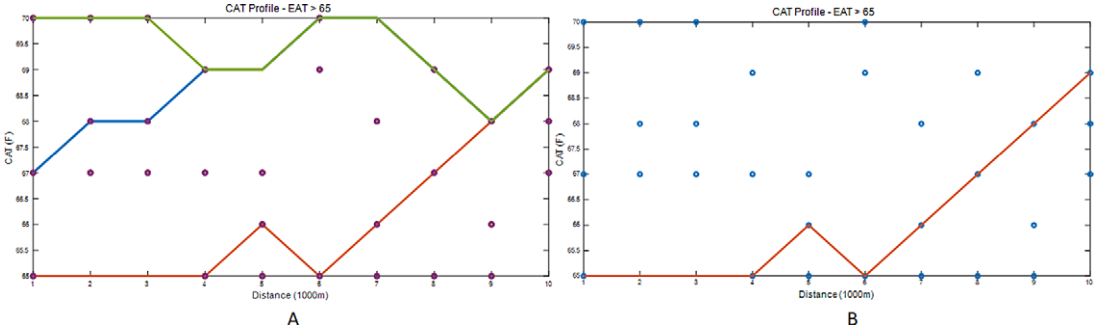

Figure 8. *Unique CATSP generation—(a) AVC = [65 70]°F and (b) Initial CAT = 65°F.*

The performance of the predicted and constant [ACCSSP, CATSP] was compared using the parameters defined in Section 4: vehicle engine performance criteria, whose output was presented in Tables 9 and 10.

The computational methods adopted in this research were quantified using a new-fangled precise approach by estimating instantaneous engine efficiency (IEE) (n_e) and smoothness measure vector (SMV) of instantaneous engine maps (IEM), along with [IFCR 1E-8 m^3/s, distance (m)] for constant and predicted [ACCSSP, CATSP] whose outcome was shown in Supplementary Figures S38–S42 and Table 11. The ratio of power output and rate of energy input was calculated to estimate IEE (Equation (12)) (mean, deviation, variance), assuming the fuel used is gasoline and its properties [calorific value (C_v), density (ρ_f)] were unchanged with the effect of temperature and pressure (Ahmed and Bhatti, 2010). The IEM was plotted on a two-dimensional plane using [IET (Nm), IES (rad/s)], and SMV was measured using the criteria defined in Section 4.4:

$$n_e = \frac{IET \cdot IES}{C_v \cdot \rho_f \cdot IFCR}. \tag{12}$$

8. Discussion

In this research, multiple engineering concepts were utilized to develop the concept of IVDM. The steps included real-time testing and Controller area network (CAN) data acquisition, developing the DL predictive models, feature functionality of vehicle engine performance, empirical methods to estimate VLV for future time steps, and iterative analysis to predict the DBV.

https://doi.org/10.1017/dce.2022.15 Published online by Cambridge University Press

Table 9. *Performance analysis—Prediction of ACCSSP.*

Parameter	ACC = 30 MPH		ACC = 40 MPH		ACC = 50 MPH		ACC = 60 MPH		ACC = 70 MPH	
Criteria	Constant	Predicted	Constant	Predicted	Constant	Predicted	Constant	Predicted	Constant	Predicted
Performance vectors										
Distance	3.00E+04	3.02E+04	4.00E+04	4.10E+04	5.00E+04	5.04E+04	5.99E+04	6.09E+04	6.99E+04	6.94E+04
IET	2.05E+05	2.05E+05	1.60E+05	1.60E+05	2.30E+05	2.30E+05	2.49E+05	2.49E+05	2.45E+05	2.45E+05
IES	2.84E+05	2.84E+05	1.39E+05	1.39E+05	1.66E+05	1.66E+05	1.69E+05	1.69E+05	2.39E+05	2.39E+05
IFCR	5.63E+05	5.62E+05	2.26E+05	2.26E+05	3.53E+05	3.53E+05	4.26E+05	4.27E+05	5.90E+05	5.90E+05
ETC	4.06E+02	4.06E+02	7.13E+02	7.12E+02	6.61E+02	6.62E+02	5.93E+02	5.93E+02	4.09E+02	4.09E+02
ESC	1.44E+03	1.44E+03	8.65E+02	8.67E+02	7.21E+02	7.21E+02	6.85E+02	6.84E+02	1.94E+03	1.90E+03
ED	4.68E+05	4.68E+05	1.27E+05	1.27E+05	2.66E+05	2.66E+05	3.42E+05	3.42E+05	5.08E+05	5.08E+05
Performance vectors—Conformance (Predicted—Constant)										
Distance	199.000		999.500		400.000		999.000		−499.000	
IET	−223.508		−74.710		−56.149		53.121		−18.207	
IES	−54.606		284.891		2.013		−59.833		20.534	
IFCR	−803.247		171.972		−95.391		33.725		−147.311	
ETC	−0.043		−0.906		0.064		−0.036		0.198	
ESC	3.071		2.158		0.176		−0.396		−33.250	
ED	−792.187		161.953		−107.700		45.969		−222.340	
Smoothness measure—R^2										
IET	0.997	0.997	0.999	0.999	0.995	0.995	0.999	0.999	0.999	0.999
IES	0.999	0.999	0.999	0.999	0.999	0.999	0.979	0.979	0.999	0.999
IFCR	0.998	0.998	0.972	0.972	0.989	0.989	0.992	0.992	0.998	0.998
ETC	0.996	0.996	0.970	0.971	0.987	0.987	0.979	0.979	0.992	0.992
ESC	0.995	0.995	0.998	0.998	0.999	0.999	0.997	0.997	0.998	0.998
ED	0.998	0.998	0.972	0.972	0.990	0.990	0.993	0.993	0.998	0.998
Smoothness measure—Adj. R^2										
IET	0.993	0.993	0.996	0.996	0.988	0.987	0.998	0.998	0.998	0.998
IES	0.996	0.996	0.998	0.997	0.999	0.999	0.948	0.947	0.998	0.998
IFCR	0.995	0.995	0.929	0.930	0.973	0.973	0.981	0.981	0.995	0.995
ETC	0.991	0.991	0.926	0.927	0.968	0.968	0.947	0.947	0.981	0.981

Continued

Table 9. *Continued*

Parameter	ACC = 30 MPH		ACC = 40 MPH		ACC = 50 MPH		ACC = 60 MPH		ACC = 70 MPH	
Criteria	Constant	Predicted	Constant	Predicted	Constant	Predicted	Constant	Predicted	Constant	Predicted
ESC	0.988	0.989	0.994	0.994	0.998	0.998	0.993	0.993	0.995	0.995
ED	0.995	0.995	0.930	0.931	0.974	0.974	0.984	0.984	0.994	0.994
Smoothness measure—SSE										
IET	8.26E+03	8.22E+03	74.064	72.920	570.321	572.589	6.47E+02	6.50E+02	3.52E+03	3.51E+03
IES	8.82E+03	8.88E+03	14.117	15.934	91.594	90.776	1.10E+03	1.11E+03	14.170	14.635
IFCR	9.94E+04	9.96E+04	1.60E+04	1.58E+04	2.44E+04	2.46E+04	4.95E+04	4.92E+04	5.75E+04	5.77E+04
ETC	0.074	0.074	0.152	0.150	0.085	0.085	0.089	0.088	0.041	0.041
ESC	1.045	1.019	0.002	0.002	0.004	0.004	0.013	0.013	53.374	46.723
ED	9.90E+04	9.91E+04	1.58E+04	1.56E+04	2.24E+04	2.25E+04	4.62E+04	4.59E+04	5.43E+04	5.45E+04
Smoothness measure—RMSE										
IET	4.535	4.524	0.429	0.426	1.191	1.194	1.269	1.272	2.960	2.957
IES	4.685	4.701	0.187	0.199	0.477	0.475	1.653	1.662	0.188	0.191
IFCR	15.730	15.741	6.301	6.263	7.795	7.819	11.096	11.061	11.958	11.983
ETC	0.014	0.014	0.019	0.019	0.015	0.015	0.015	0.015	0.010	0.010
ESC	0.051	0.050	0.002	0.002	0.003	0.003	0.006	0.006	0.364	0.341
ED	15.698	15.708	6.270	6.233	7.468	7.492	10.725	10.691	11.621	11.646

Table 10. *Performance analysis—Prediction of CATSP.*

Parameter	EAT (°F)	CAT (°F)	Area	Conformance	R^2	Adj. R^2	SSE	RMSE
ACCSSP = 30 MPH								
EST	82.076	69	412.431	−66.097	0.936	0.841	28.869	0.858
(A1 + A2)		Predicted	346.334		0.803	0.506	223.958	2.391
	37.985	70	695.211	−0.457	0.989	0.971	13.008	0.576
		Predicted	694.754		0.989	0.972	13.015	0.576
ACRFP (B)	82.076	69	4,796.364	−271.024	0.991	0.978	596.296	3.901
		Predicted	4,525.340		0.988	0.969	703.936	4.239
	37.985	70	28,447.657	−12.325	0.992	0.980	8.751	0.473
		Predicted	28,435.331		0.992	0.980	8.755	0.473
ACCSSP = 40 MPH								
EST	85.289	68	269.142	0.051	0.951	0.878	16.910	0.657
(A1 + A2)		Predicted	269.193		0.963	0.907	12.982	0.576
	37.634	71	429.335	−37.710	0.991	0.977	7.832	0.447
		Predicted	391.625		0.990	0.975	9.661	0.497
ACRFP (B)	85.289	68	5,992.344	−550.425	0.968	0.919	447.093	3.378
		Predicted	5,441.919		0.974	0.935	367.982	3.065
	37.634	71	28,028.615	−6.797	0.988	0.970	18.523	0.688
		Predicted	28,021.818		0.988	0.970	18.590	0.689
ACCSSP = 50 MPH								
EST	80.726	67	561.773	2.441	0.962	0.905	7.244	0.430
(A1 + A2)		Predicted	564.214		0.959	0.898	7.967	0.451
	40.1	72	876.469	−1.070	0.885	0.713	1.246	0.178
		Predicted	875.399		0.884	0.709	1.252	0.179
ACRFP (B)	80.726	67	1,904.872	59.813	0.981	0.952	382.367	3.124
		Predicted	1,964.686		0.983	0.957	351.031	2.993
	40.1	72	28,276.442	0.118	0.980	0.951	0.613	0.125
		Predicted	28,276.559		0.980	0.951	0.613	0.125
ACCSSP = 60 MPH								
EST	79.44	66	738.825	−192.196	0.961	0.902	13.422	0.585
(A1 + A2)		Predicted	546.629		0.957	0.893	17.459	0.668
	38.858	73	783.449	−3.056	0.981	0.953	4.052	0.322

Continued

https://doi.org/10.1017/dce.2022.15 Published online by Cambridge University Press

Table 10. *Continued*

Parameter	EAT (°F)	CAT (°F)	Area	Conformance	R^2	Adj. R^2	SSE	RMSE
		Predicted	780.393		0.982	0.954	4.099	0.323
ACRFP	79.44	66	8,978.425	−2,153.683	0.909	0.772	13.125	0.579
(B)		Predicted	6,824.742		0.993	0.982	669.514	4.134
	38.858	73	28,658.279	1.219	0.988	0.970	0.004	0.010
		Predicted	28,659.498		0.991	0.977	0.004	0.010
ACCSSP = 70 MPH								
EST	76.1	65	1,427.487	−904.718	0.990	0.976	1.027	0.162
(A1 + A2)		Predicted	522.768		0.997	0.993	5.569	0.377
	36.518	74	118.232	−10.842	0.934	0.835	2.274	0.241
		Predicted	107.390		0.944	0.861	2.069	0.230
ACRFP	76.1	65	1,433.399	253.377	0.862	0.655	6,501.550	12.882
(B)		Predicted	1,686.776		0.873	0.681	6,049.353	12.426
	36.518	74	28,851.815	2.671	0.806	0.514	0.000	0.003
		Predicted	28,854.486		0.980	0.950	0.000	0.002

Table 11. *Quantification of IVDM — IEE and IEM.*

Test cases		IEE			IEM			Performance	
Speed (MPH)	Profile	Mean	Deviation	Variance (1E-3)	R^2	Adj R^2	RMSE	IFCR (1E-3 m^3)	Distance (1E+5 m)
30	Constant	0.3210	0.0424	0.0018	0.9968	0.7878	12.4481	4.7716	0.1338
	Predicted	0.3180	0.0415	0.0017	0.9983	0.8956	8.6682	4.7857	0.1401
40	Constant	0.3256	0.0281	0.7898	0.9998	0.9966	1.3902	3.4894	0.1785
	Predicted	0.3254	0.0281	0.7870	0.9999	0.9982	1.0034	3.4882	0.1811
50	Constant	0.3320	0.0313	0.001	0.9981	0.9560	5.1152	3.7634	0.2231
	Predicted	0.3339	0.0317	0.001	0.9961	0.9425	5.8793	3.7477	0.2146
60	Constant	0.3295	0.0286	0.8164	0.9964	0.7411	10.3102	3.8386	0.2677
	Predicted	0.3298	0.0286	0.8204	0.9933	0.8836	6.9115	3.8330	0.2628
70	Constant	0.3154	0.0221	0.4889	0.9991	0.9900	0.6721	3.6281	0.3123
	Predicted	0.3138	0.0219	0.4817	0.9998	0.9964	0.4067	3.6415	0.3181

The constant and predicted [ACCSSP, CATSP] were generated based on the developed concepts as shown in Supplementary Figures S28–S37, for the selected snippets of Speeds and CAT ranging [30 70] MPH) and [65 75]°F. Definite values were selected as the [Initial ACC Speed, Initial CAT] to generate a unique [ACCSSP, CATSP], and the performance analysis corresponding to the vehicle engine performance criteria were shown in Tables 9 and 10. The SMV for constant and predicted [ACCSSP, CATSP] were interpreted, and it was observed that in most cases, the performance was similar. The criteria for SMV was defined in Supplementary Table S11, and in 35% of the cases predicted [ACCSSP, CATSP] has higher [R^2 Adj. R^2] and lower [SSE RMSE], whereas 50% of the scenarios scored the same.

Among all the parameters (Section 4), the most critical elements of interest for vehicle engine performance are [IFCR, 1E-8 m^3/s), Distance], and the conformance of predicted and constant ACCSSP test cases are shown in Table 9. The predicted ACCSSP with the snippet speed = [30 50] MPH resulted in lower IFCR by [803.247 95.391], with an additional distance traversed by [199 400] m. The constant ACCSSP with speed = [70] MPH, resulted in higher IFCR [147.311], ED [222.34], distance [499] m, and lower [ESC, ETC] = [20.54, 0.198] which depicts vehicle movement on higher-gradient terrain. The algorithm developed for this work also allots priority to lowering the trip time, and hence the predicted ACCSSP with speed snippet = [40 60] MPH resulted in higher distance = [999.5 999] m and IFCR = [171.972, 33.725].

Similarly, the performance of the predicted and constant [CATSP] was analyzed by the conformance vectors [Engine surface temperature (EST), ACRFP] = [A1 + A2, B] as shown in Table 10. The two test scenarios with EAT ≥ 65°F and EAT <45°F were investigated, and lower values of the area [A1 + A2] (EST) and B (ACRFP) are desired for enhanced HVAC performance. In the test case scenario with ACCSSP = 70 MPH, the predicted CATSP with EAT = [76.1 36.5]°F, resulted in lower EST by [904.718, 10.842]. However, the ACRFP has higher magnitudes for the predicted CATSP, which is compensated by the better SMV similar to the snippet with ACCSSP = 50 MPH. The [EST, ACRFP] for predicted CATSP are higher by 2.441 and 59.813 for EAT = 80.72°F, which is not desirable. But the SMV of ACRFP for the predicted CATSP has higher [R^2, Adj. R^2] = [0.983 0.957] and lower [SSE RMSE] = [351.03 2.993]. Similarly, for EAT = 40.1°F, the EST for the constant CATSP is higher by 1.07, and the rest of the criteria have comparable values. Thus, enhanced performance was concluded by analyzing the vehicle engine performance parameters for the test cases with ACCSSP = [30, 40, 60] MPH.

https://doi.org/10.1017/dce.2022.15 Published online by Cambridge University Press

Additionally, the efficacy of IVDM was quantified by estimating the instantaneous engine efficiency (IEE), smoothness measure vector (SMV) of instantaneous engine maps (IEM), and [IFCR, Distance] for another set of snippets selected in a similar speed range [30 70] MPH. The plots and analytical results were depicted in Supplementary Figures S38–S42 and Table 11. The SMV criteria defined in Section 4.4 was adopted for IEM, whereas higher IEE [mean] and lower IEE [Deviation, variance] are desired for optimal vehicle engine performance. It was observed that the IEM RMSE of the predicted ACCSSP has lower values than the constant ACCSSP for all the test cases except for ACCSSP = 50 MPH, where the RMSE = [5.115 5.879] share similar magnitudes. The test case with constant ACCSSP = 30 MPH has a lower IFCR = 4.77, but the vehicle traverses additionally 630 m with predicted ACCSSP. The IEE [mean, variance] for constant ACCSSP = 40 MPH were [0.3256, 0.7898E-3], and the predicted ACCSSP scored [0.3254, 0.787E-3]. Thus IEE [variance] of the predicted ACCSSP is lower, and the IEE [mean, Deviation] shares similar values. This approach of analyzing the [IEE, IEM] was not discussed in the existing literature, and the computational results were assumed to be satisfactory. Therefore, overall observation resulted that predicted ACCSSP satisfies the desired criteria in most of the scenarios and best confirms the validation of the proposed IVDM.

The analytic results depicted IVDM ameliorates vehicle engine performance by predicting [ACCSSP, CATSP] optimizing [EOP, CATOP]. The results obtained were good, and IVDM could emerge as a significant feature in automotive systems.

9. Conclusion

This research proposed a novel drive mode named "intelligent vehicle drive mode" (IVDM), which augments the vehicle engine performance in real-time without increasing the trip time under normal driving conditions. The IVDM is not currently integrated into any vehicle segment and predicts the DBV (speed, LOT, LAT, YAR, CAT] by optimizing the vectors [EOP, CATOP], obliging the driver's command in real-time. The IVDM activates the ACC feature when triggered; thus, LOT is automatically determined by the ACC controller, and the parameters [LAT, YAR] were estimated by the defined mathematical models assuming ideal steering behavior (ISB). The prediction of [ACCSSP, CATSP] was made by applying the optimal Engine operating conditions criteria on the predicted parameters [EOP, CATOP]. Autoregressive network with exogenous inputs (NARX) DL models were developed to map the VLV and [EOP, CATOP], whose performance was validated using the traditional statistical measure vector (STMV). The quantification of the computational model was performed by comparing the Engine operating conditions parameters for constant and predicted [ACCSSP, CATSP] and analyzing the [IEE, IEM] using the single test vehicle 2020 Cadillac CT5. The results were satisfactory, and this concept could be utilized to develop a new feature in the vehicle.

10. Future Work

The computational model of intelligent vehicle drive mode (IVDM) validated the vehicle engine performance criteria using the elements [EOP, CATOP] for internal combustion engine-driven segment with a single test vehicle, 2020 Cadillac CT5, under normal driving conditions. As future work, the validation could be enhanced, including multiple vehicle lines, conducting tests for critical scenarios of mountain regions (>14% slope), considering slip and extreme weather conditions (EAT > 85°F or EAT <25°F). In this research, the environmental factors [humidity (HUM), atmospheric pressure (ATP)], HVAC elements (engine fan speed, power, Nusselt number), the sensitivity of gasoline properties [calorific value (C_v), density (ρ_f)] due to pressure and temperature changes, and constant CATSP to predict ACCSSP were assumed to simplify the analytical approach. Also, in this research, built-in MATLAB functions with default properties were utilized to develop deep learning (DL) models. Therefore, the analysis can be extended incorporating all the affecting parameters and customized DL models could be developed for each vehicle model data to enhance prediction precision. Also, the optimal performance criteria were defined with basic relations between the parameters [EOP, CATOP] to simplify

https://doi.org/10.1017/dce.2022.15 Published online by Cambridge University Press

the analysis, thus enhanced vehicle engine performance criteria, including additional Engine and powertrain parameters, would produce improved results.

The fail-soft action was implemented to generate unique [ACCSSP, CATSP], which produced satisfactory results of augmented Engine operating conditions. However, the generated profile might not be the only optimal solution, and basic iterative analysis was adopted to estimate [eligible vehicle speeds (MPH), eligible vehicle cabin air temperatures (°F)]; further research could be adopted to ameliorate the results by developing an enhanced algorithm (e.g., reinforcement model adapting the driver behavior). Also, the concept of IVDM could be extended with new criteria for road segments of either parking lots, low curvatures (RRC = [8.34 42.57]m), or arterial roads (vehicles speed <25 MPH) whose effect on Engine operating conditions is insignificant.

The feature development is a multistage process, and as the next step of this work, the plant simulation model controls algorithm and software integration followed by validation could be deployed. The emergence of electric and autonomous vehicles has triggered a new research path for the automotive sector in recent years. Hence, IVDM could be developed for electric vehicles by defining new performance criteria for (battery operating point, motor operating point), which enhances the operating conditions of (battery, inverter, motor), and substantial validation can be performed with multiple test vehicle segments to enhance the efficacy of the proposed concept. Also, an interface could be developed between IVDM and integrated path planning and perception algorithms of autonomous systems to enhance driving behavior.

Acknowledgments. The authors would like to thank Iqbal Surti and Michael Mati, Systems Engineers, for their assistance in real-time testing, Curtis L. Hay, Technical Specialist, for his inputs, and Tanzima Mushtarin, Lead Engineer, for continuous support throughout the period at General Motors Inc., Warren, Michigan. The technical analysis was performed using the tools provided by General Motors Inc., Warren, Michigan (Vehicle Spy and neoVI—Fire 2) and the University of Michigan (MATLAB). The authors also appreciate Dr Hariharan Venkitachalam, Karthik Reddy Vemireddy, Mustafa Mudassir Mohammad, Dr Ramakrishnan Ambur Sankaranarayanan, and Abhishek Sundaresan from RWTH Aachen University, Germany, for participating in initial discussions.

Supplementary Materials. To view supplementary material for this article, please visit http://doi.org/10.1017/dce.2022.15.

Data Availability Statement. The data used in this work are proprietary to General Motors Inc., Warren, Michigan, and further details cannot be made publicly available. However, the modeling algorithm is available on request.

Author Contributions. Srikanth Kolachalama came up with the idea, developed the concept, and performed the analysis. Dr. Hafiz Malik is the principal investigator for this project.

Funding Statement. The project "Intelligent Vehicle Drive Mode–Predictive Model of Driver Behaviour Vector," was performed under the research collaboration of the University of Michigan and General Motors Inc.,Warren, Michigan funded by William J. Clifford (Director) and Matthus W. Joshua (Executive Director) of the Systems Engineering Department at General Motors Inc., Warren, Michigan.

Competing Interests. The authors declare no competing interests exist.

References

Ahmed Q and Bhatti AI (2010) Estimating SI engine efficiencies and parameters in second-order sliding modes. *IEEE Transactions on Industrial Electronics 58*(10), 4837–4846.

Baldacci R, **Battarra M and Vigo D** (2008) Routing a heterogeneous fleet of vehicles. In *The Vehicle Routing Problem: Latest Advances and New Challenges*. Boston, MA: Springer, pp. 3–27.

Boggio-Marzet A, **Monzon A**, **Rodriguez-Alloza AM and Wang Y** (2021) Combined influence of traffic conditions, driving behavior, and type of road on fuel consumption. Real driving data from Madrid area. *International Journal of Sustainable Transportation 17*(1), 1–13.

Borman G and Nishiwaki K (1987) Internal-combustion engine heat transfer. *Progress in Energy and Combustion Science 13*(1), 1–46.

Cariou C, **Lenain R**, **Thuilot B and Berducat M** (2008) Automatic guidance of a four-wheel steering vehicle. In *66th LandTechnik Conference: Agricultural Engineering*. Düsseldorf: VDI Verlag GmbH, p. 6.

Chau CK, **Elbassioni K and Tseng CM** (2016) Fuel minimisation of plug-in hybrid electric vehicles by optimising drive mode selection. In *Proceedings of the Seventh International Conference on Future Energy Systems*, Waterloo, Canada, pp.1–11, Association for Computing Machinery, NewYork, NY USA.

Chau CK, **Elbassioni K and Tseng CM** (2017) Drive mode optimisation and path planning for plug-in hybrid electric vehicles. *IEEE Transactions on Intelligent Transportation Systems 18*(12), 3421–3432.

Chen Z, **Li X and Zhou X** (2019) Operational design for shuttle systems with modular vehicles under oversaturated traffic: Discrete modeling method. *Transportation Research Part B: Methodological 122*, 1–19.

Davis B (2019) *Teen Driver Support System Technology Transfer, Center for Transportation Studies*. Minneapolis, MN: University of Minnesota.

Dietsche KH and Kuhlgatz D (2014) History of the automobile. In *Fundamentals of Automotive and Engine Technology*. Wiesbaden: Springer Vieweg, pp. 1–7.

Eathakota VP, **Kolachalama S**, **Krishna KM and Sanan S** (2008) Optimal posture control for force actuator based articulated suspension vehicle for rough terrain mobility. *Advances in Mobile Robotics*, 760–767.

Eathakota V, **Singh AK**, **Kolachalam S and Krishna KM** (2010) Determination of optimally stable posture for force actuator based articulated suspension for rough terrain mobility. In *FIRA RoboWorld Congress*. Berlin: Springer, pp. 154–161.

Gao Z, **Smith DE**, **Daw CS**, **Edwards KD**, **Kaul BC**, **Domingo N**, **Parks JE and Jones PT** (2015) The evaluation of developing vehicle technologies on the fuel economy of long-haul trucks. *Energy Conversion and Management 106*, 766–781.

Goodarzi A and Esmailzadeh E (2007) Design of a VDC system for all-wheel independent drive vehicles. *IEEE/ASME Transactions on Mechatronics 12*(6), 632–639.

Gusev SV, **Johnson W and Miller J** (1997). Active flywheel control based on the method of moment restrictions. In *Proceedings of the 1997 American Control Conference (Cat. No. 97CH36041)*, vol. 5. Albuquerque, NM: IEEE, pp. 3426–3430.

Hac A, **Fulk D and Chen H** (2008) Stability and control considerations of vehicle-trailer combination. *SAE International Journal of Passenger Cars-Mechanical Systems 1*, 925–937.

Jaynes M, **Dantu R**, **Varriale R and Evans N** (2016). Automating ECU identification for vehicle security. In *2016 15th IEEE International Conference on Machine Learning and Applications (ICMLA)*. Anaheim, CA: IEEE, pp. 632–635.

Johansson KH, **Törngren M and Nielsen L** (2005). Vehicle applications of controller area network. In *Handbook of Networked and Embedded Control Systems*. Boston: Birkhäuser, pp. 741–765.

Kakaee AH, **Shojaeefard MH and Zareei J** (2011) Sensitivity and effect of ignition timing on the performance of a spark-ignition engine: An experimental and modeling study. *Journal of Combustion 2011*, 1–8.

Kolachalama S, **Hay CL**, **Mushtarin T**, **Todd N**, **Heitman J and Hermiz S** (2018) *An Algorithm to Estimate Steering Behavior Using Vehicle Radius of Curvature, 647068, Research Disclosure*. Paris: Questel Ireland.

Kolachalama S, **Kuppa K**, **Mattam D and Shukla M** (2008) Thermal analysis of radiator core in heavy duty automobile. *ASME Heat Transfer Summer Conference*, vol. 48487, pp. 123–127, Jacksonville, Florida, USA.

Kolachalama S and Lakshmanan S (2021) *Using Deep Learning to Predict the Engine Operating Point in Real-Time (No. 2021-01-0186)*. SAE Technical Paper.

Kolachalama S and Malik H (2021a) Predictive model of adaptive cruise control speed to enhance engine operating conditions. *Vehicles 3*(4), 749–763.

Kolachalama S and Malik H (2021b) A NARX model to predict cabin air temperature to ameliorate HVAC functionality. *Vehicles 3*(4), 872–889.

Labuhn PI and Chundrlik WJ (1995) *US Patent No. 5,454,442*. Washington, DC: US Patent and Trademark Office.

Lairenlakpam R, **Jain AK**, **Gupta P**, **Kamei W**, **Badola R and Singh Y** (2018) *Effect of Real-World Driving and Different Drive Modes on Vehicle Emissions and Fuel Consumption* (*No. 2018-01-5017)*. SAE Technical Paper.

Liang C, **Ji L**, **Mousavi H and Sandu C** (2019) Evaluation of tire traction performance on dry surface based on tire-road contact stress. In *SIAR International Congress of Automotive and Transport Engineering: Science and Management of Automotive and Transportation Engineering*. Cham: Springer, pp. 138–152.

Luo LH, **Liu H**, **Li P and Wang H** (2010) Model predictive control for adaptive cruise control with multi-objectives: Comfort, fuel economy, safety and car-following. *Journal of Zhejiang University Science A 11*(3), 191–201.

Marsden G, **McDonald M and Brackstone M** (2001) Towards an understanding of adaptive cruise control. *Transportation Research Part C: Emerging Technologies 9*(1), 33–51.

Melman T, **de Winter J**, **Mouton X**, **Tapus A and Abbink D** (2021) How do driving modes affect the vehicle's dynamic behaviour? Comparing Renault's multi-sense sport and comfort modes during on-road naturalistic driving. *Vehicle System Dynamics 59*(4), 485–503.

Onder CH and Geering HP (1995) *Model-Based Engine Calibration for Best Fuel Efficiency*, vol. 950983. SAE Technical Paper.

Paul A, **Chauhan R**, **Srivastava R and Baruah M** (2016) *Advanced Driver Assistance Systems (No. 2016-28-0223)*. SAE Technical Paper.

Sharma A, **Singh J and Kumar A** (2015) Optimum design and material selection of Baja vehicle. *International Journal of Current Engineering and Technology 5*(3), 2169–2180.

Sturgeon TJ, **Memedovic O**, **Van Biesebroeck J and Gereffi G** (2009) Globalisation of the automotive industry: Main features and trends. *International Journal of Technological Learning, Innovation and Development 2*(1–2), 7–24.

Sudin MN, **Abdullah MA**, **Shamsuddin SA**, **Ramli FR and Tahir MM** (2014) Review of research on vehicles aerodynamic drag reduction methods. *International Journal of Mechanical and Mechatronics Engineering 14*(2), 37–47.

https://doi.org/10.1017/dce.2022.15 Published online by Cambridge University Press

Taghavifar H and Mardani A (2017) Off-road vehicle dynamics. *Studies in Systems, Decision and Control 70*, 37.

Wåhlberg AE (2007) Long-term effects of training in economical driving: Fuel consumption, accidents, driver acceleration behavior and technical feedback. *International Journal of Industrial Ergonomics 37*(4), 333–343.

Zhang X and Mi C (2011) *Vehicle Power Management: Modeling, Control and Optimisation*. Berlin: Springer Science & Business Media.

Zoepf SM (2011). *Automotive Features: Mass Impact and Deployment Characterisation*. Cambridge, MA: Massachusetts Institute of Technology.

Zoepf S and Heywood JB (2012) Characterisations of deployment rates in automotive technology. *SAE International Journal of Passenger Cars-Electronic and Electrical Systems 5*, 541–552.

Zou Y, **Sun F**, **Hu X**, **Guzzella L and Peng H** (2012) Combined optimal sizing and control for a hybrid tracked vehicle. *Energies 5* (11), 4697–4710.

Cite this article: Kolachalama S and Malik H (2022). Intelligent vehicle drive mode which predicts the driver behavior vector to augment the engine performance in real-time. *Data-Centric Engineering*, 3, e14. doi:10.1017/dce.2022.15